Emergence of Multiscale Dynamics in Colloidal Gels: Supplemental Material

Jae Hyung Cho,[1] Roberto Cerbino,[2] and Irmgard Bischofberger[1]

[1] *Department of Mechanical Engineering, Massachusetts Institute of Technology, Cambridge, Massachusetts 02139, USA*
[2] *Dipartimento di Biotecnologie Mediche e Medicina Traslazionale, Università degli Studi di Milano, Via. F.lli Cervi 93, Segrate (MI) I-20090, Italy*

(Dated: February 27, 2020)

1. Particle synthesis and characterization

For the first part of the synthesis of the polystyrene-poly(N-isopropylacrylamide) (PS-PNIPAM) core-shell particles, we follow the protocol described in Ref. [1], which is slightly modified from that of Ref. [2]. In a 1 L flask equipped with a stirrer, a reflex condenser, and a gas inlet, 25.02 g of N-isopropylacrylamide (NIPAM, Acros Organics) and 0.2008 g of the stabilizer sodium dodecyl sulfate (SDS, Sigma-Aldrich) are dissolved in 525.14 g of DI water. After the solution is bubbled with nitrogen for 30 min, 142.75 g of styrene (Sigma-Aldrich) is added, and the mixture is heated to 80°C in nitrogen atmosphere. Then 0.3521 g of the initiator potassium persulfate (KPS, Acros Organics) dissolved in 15.00 g of DI water is added to the mixture. After 6 h, the dispersion is cooled to room temperature and cleaned through repeated centrifugation and supernatant exchange.

For the second part, we use the seeded emulsion polymerization in Ref. [2] that increases the thickness of the PNIPAM shell, with slight modification of the ratio of the materials. For each 100 g of the particles obtained from the first part, 12.58 g of NIPAM and 0.8994 g of the crosslinker N,N'-methylenebis(acrylamide) (BIS, Sigma-Aldrich) are added, and the mixture is heated to 80°C. After the addition of 0.1264 g of KPS dissolved in 9.43 g of DI water, the mixture is stirred for 4 h. The suspension is then cooled to room temperature, and cleaned by dialysis against DI water for approximately 4 weeks.

We add sodium thiocyanate (NaSCN) to screen the charges of the synthesized particles. To probe the amount of NaSCN necessary to neglect the range of electrostatic repulsions, we gradually increase the concentration c of NaSCN and measure the viscoelastic moduli of the resulting gels at the temperature T = 30°C. We observe that the moduli gradually increase with c, until they remain constant in the range of $c = 0.3 - 0.7$ M. Hence we conduct all of our experiments at $c = 0.5$ M.

We estimate the value of the gelation temperature T_g by measuring T, at which the storage modulus G' becomes larger than the loss modulus G'', during a temperature ramp experiment at the ramp rate of 0.2 °C/ min that is sufficiently slow to ensure uniform sample temperature [1]. We estimate the interparticle attraction strength at T = 30°C to be $\sim 3.5\ k_BT$, where k_B is the Boltzmann constant, from the dependence of G' on the particle volume fraction ϕ, using the van der Waals potential [1]. Yet, we expect strong influence of noncentral forces between neighboring particles on the rheological properties of our gels, which would effectively lead to a larger attraction strength.

We measure the radius of gyration r_g of a particle to be 81.4 ± 0.7 nm at 30°C and 82.3 ± 0.9 nm at 20°C by using the Guinier plot via static light scattering, which corresponds to a hard sphere radius $r = \sqrt{5/3}r_g$ of r = 105.1 ± 1.0 nm at 30°C and r = 106.2 ± 1.2 nm at 20°C. In addition, we measure the hydrodynamic radius a to be 116.3 ± 1.8 nm at 30°C and 139.9 ± 1.7 nm at 20°C by using the Stokes-Einstein relation via dynamic light scattering. Due to the sparse, brush-like structure of the PNIPAM shell [2], r is expected to represent the approximate radius of the dense PS core, as evidenced by the small T-dependence of r. The hydrodynamic radius a is expected to overestimate the actual radius of the entire core-shell particle, as the Stokes drag assumes a perfect, smooth sphere. We thus infer a negligible thickness of the PNIPAM shell compared to the size of the PS core, and use the density of polystyrene ρ = 1.05 g/cm^3 to estimate ϕ from the mass change of a sample after drying it in an oven.

2. Rheological measurements

For the measurement of the storage modulus G', we use an AR-G2 rheometer (TA Instruments) to perform small amplitude oscillatory shear experiments. For each sample, upon a sudden temperature increase from 20°C to 30°C at time t = 0 s, we monitor the temporal evolution of the viscoelastic moduli during a time sweep. When the change in the moduli becomes very slow at $t \approx 2400$ s, an amplitude sweep is followed (for samples at low ϕ, the time sweep is prolonged until $t \approx 4200$ s to account for the slower kinetics). The values of G' reported are the mean values within the linear range (strain amplitude $\gamma_0 \approx 0.001 - 0.1$), where the moduli are constant. We use a 40 mm cone-plate geometry, and all the experiments are performed at the frequency f = 1 Hz.

3. Curve-fitting method

The image structure function $D(q,\Delta t)$ computed with the DDM algorithm can be expressed as

$$D(q,\Delta t) = A(q)\,(1 - f(q,\Delta t)) + B(q), \tag{1}$$

where $A(q)$ is determined by optical properties of the microscope and static information about the sample, and $B(q)$ represents the level of the camera noise [3]. The form of the normalized intermediate scattering function we assume is

$$f(q,\Delta t) = (1 - C(q))\exp\left[-\left(\frac{\Delta t}{\tau(q)}\right)^{p(q)}\right] + C(q), \tag{2}$$

where $C(q)$ is the nonergodicity parameter, Δt the delay time, $\tau(q)$ the relaxation time, and $p(q)$ the stretching exponent. We determine $A(q)$ and $B(q)$ prior to the curve-fitting. The value of $B(q)$ is independent of the wave vector q if the detection noise of the camera is uncorrelated in space and time [4]. Indeed we observe that $D(q,\Delta t)$ becomes independent of both q and Δt in the highest-q domain accessible ($q > 9.5$ µm^{-1} for the 20× objective and $q > 28$ µm^{-1} for the 60× objective), where $A(q)$ approaches zero. We calculate the mean of $D(q,\Delta t)$ in this domain and equate the resulting value to $B(q)$.

In linear space invariant imaging, where the sample density field is linearly mapped onto the image intensity field, the ensemble-averaged squared modulus of Fourier-transformed images can be expressed as

$$\left\langle \left|\hat{i}(q)\right|^2 \right\rangle_E \simeq \frac{A(q)}{2} + \frac{B(q)}{2}, \tag{3}$$

provided that the non-ideal contributions arising from imperfections, such as scratches, stains, or dust particles, along the optical path are negligible compared to those from the sample [3]. Hence we calculate $A(q)$ from $\left\langle \left|\hat{i}(q)\right|^2 \right\rangle_E$ and $B(q)$.

We use *lsqcurvefit* in MATLAB to extract the three remaining parameters from curve-fits. We first plot $D(q,\Delta t)$ as a function of Δt in linear-log scales to estimate the time window $\Delta t = [0, \Delta t^*]$ of the fast relaxation dynamics by ensuring that a point of inflection is captured in the domain. Such a point of inflection indicates that the relaxation time $\tau(q) \lesssim \Delta t^*$, and therefore the plateau of $D(q, \Delta t \to \infty) = A(q)\,(1 - C(q)) + B(q)$, is properly captured by fitting the model to the data. The nonergodicity parameter $C(q)$ is obtained from this plateau value. To improve the reliability of the fitting values of the relaxation time $\tau(q)$ and the stretching exponent $p(q)$, we then linearize Eq. (1) with Eq. (2) by plotting $D_{lin} = \log\left(-\log\left[1 - \frac{D(q,\Delta t) - B(q)}{A(q)(1-C(q))}\right]\right)$ as a function of $\log(\Delta t)$ such that the slope is equal to $p(q)$ and the y-intercept $-p(q)\log(\tau(q))$. The resulting plot is linear for early $\log(\Delta t)$ and typically starts to show a gradually decreasing slope for later $\log(\Delta t)$. By performing linear regression to the data in the early times as shown in the insets of Fig. 1(a,b), we re-evaluate $\tau(q)$ and $p(q)$. We then use these values to plot Eq. (1) and check the quality of the resulting fit. We find that this last step of correction is crucial, as p is highly sensitive to the fitting domain of Δt. The sensitivity originates from the properties of the stretched exponential function, which inherently contains a broad distribution of constituent time scales [5]. Examples of the final fits to $D(q,\Delta t)$ and the corresponding $f(q,\Delta t)$ at the particle volume fraction $\phi = 0.8\%$ are displayed in Fig. 1. As the sample age t since the onset of aggregation increases, the curves become more stretched, while the relaxation time increases, as shown in Fig. 1(c) (same data as in Fig. 1(d) of the main text). For the aged gels, the nonergodicity parameter, as visualized by the large Δt plateau in f, decreases with q, as displayed in Fig. 1(d).

4. Measurement of the fractal dimension d_f

The static structure factor $S(q)$ is calculated by dividing the squared modulus of Fourier-transformed images of a gel by that of the same system before the initiation of gelation for each q [3, 6]. The resulting $S(q)$ in the high-q regime displays a power law with an exponent -1.8 ± 0.1, independent of time t, as shown in Fig. 2 for the particle volume fraction $\phi = 0.8\%$. We confirm that the exponent is independent of ϕ as well. The absolute value of the exponent represents the fractal dimension $d_f \approx 1.8 \pm 0.1$ [7].

At lower q, a peak appears in $S(q)$, which typically indicates the uniformity of the cluster size [7]. However, we find that $S(q)$ from our experiments is significantly influenced in the low-q domain by the optical properties of the experimental setup. Hence we use $S(q)$ only to determine d_f in the high-q domain.

5. q-independence of $p(q)$

For all t and ϕ, the stretching exponent $p(q)$ is largely independent of q, as shown in Fig. 3. We find that the level of noise increases for the low-q domain, but we nonetheless assume q-independence of p, given the robustness of the mean.

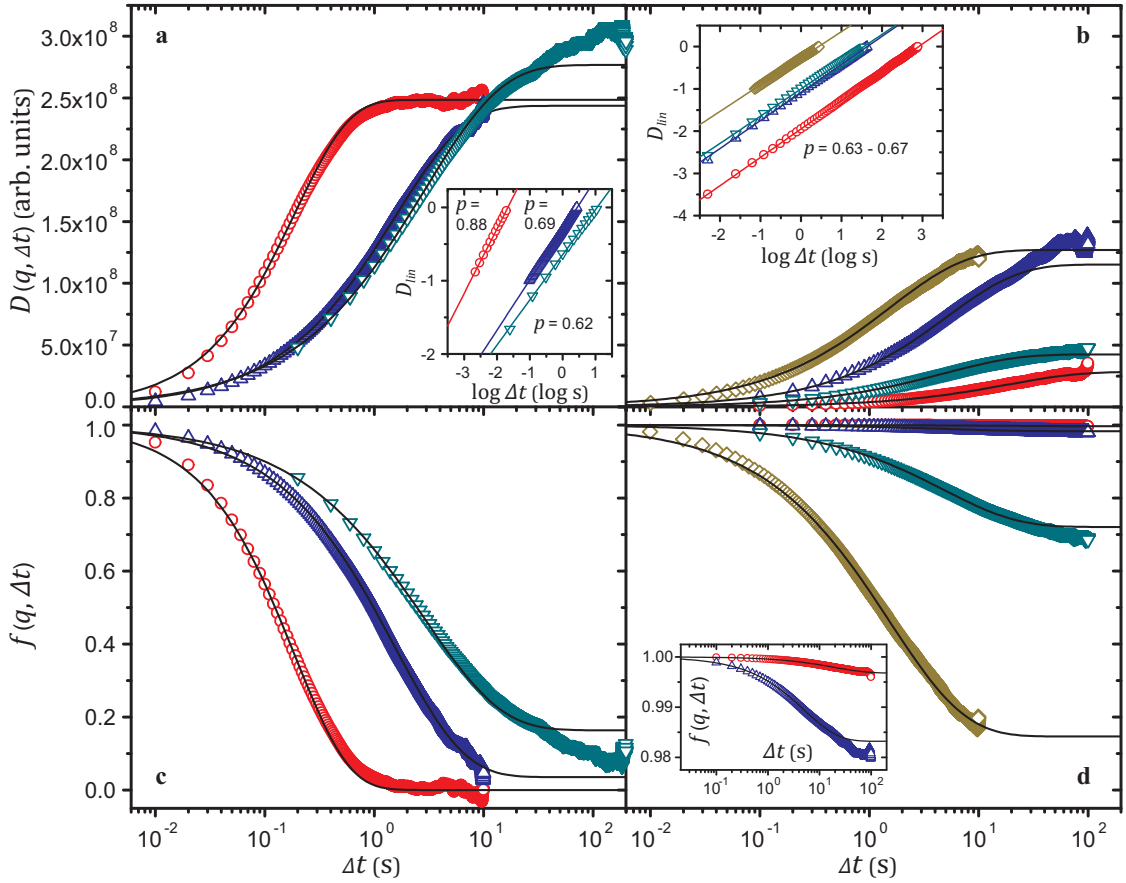

FIG. 1. Image structure function $D(q,\Delta t)$ (a, b), normalized intermediate scattering function $f(q,\Delta t)$ (c, d), and the fitting curves (black lines) for the system at particle volume fraction ϕ = 0.8%. The correlation functions in (a) and (c) correspond to the sample ages t = 180 s (○), 1500 s (△), and 3600 s (▽) at the wave vector q = 4.0 μm^{-1} or qa = 0.47, where a is the hydrodynamic radius of a particle. The correlation functions in (b) and (d) correspond to qa = 0.0088 (○), qa = 0.058 (△), qa = 0.23 (▽), and qa = 0.58 (◇) of the aged gel. Insets (a,b): linearized image structure function $D_{lin}(\log\Delta t)$, whose slope equals the stretching exponent p. Inset (d): a zoomed-in image of the curves for qa = 0.0088 (○) and qa = 0.058 (△).

6. Maximum mean squared displacement δ^2 of the clusters

We repeat Eq. (5) of the main text here for convenience:

$$f(q,\Delta t\to\infty) = \exp\left(-\frac{q^2\delta^2}{4}\right) = C(q), \tag{4}$$

where δ^2 is the maximum mean squared displacement of the clusters [8], and $C(q)$ is the nonergodicity parameter. By fitting Eq. (4) to $C(q)$ in the intermediate-q domain, where the dynamics is dominated by the clusters, as shown in Fig. 4, we extract the only free parameter δ^2. For each ϕ, Eq. (4) yields a satisfactory fit until it deviates from $C(q)$ in the high-q domain, where the internal vibrations of fractals determine $\tau(q)$. The resulting values of δ^2 as a function of ϕ obey a power law with an exponent -2.07 ± 0.04, as displayed in the inset of Fig. 4.

7. Direct application of the Krall-Weitz model

To further verify the equivalence of the dynamics in the intermediate-q regime to that of the model reported in Ref. [8], hereafter referred to as the Krall-Weitz model, we directly apply the Krall-Weitz model to fit to the image structure function $D(q,\Delta t)$ by using Eq. (3) of the main text for the normalized intermediate scattering function, repeated here [8]:

$$f(q,\Delta t) = \exp\left[-\frac{q^2\delta^2}{4}\left(1-\exp\left[-\left(\frac{\Delta t}{\tau}\right)^p\right]\right)\right]. \tag{5}$$

For both models, we use the same domains of Δt to fit to $D(q,\Delta t)$ for each q and ϕ. Because of the more complex form of the double exponentials in Eq. (5), however, we observe that τ extracted from the Krall-Weitz model is more susceptible to noise, as shown in Fig. 5. We omit τ of the Krall-Weitz model for lower values of q since the quality of the fits significantly deteriorates.

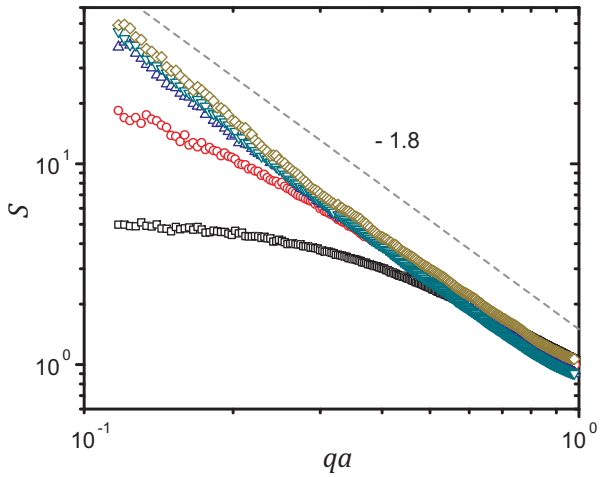

FIG. 2. Static structure factor S of the gel at $\phi = 0.8\%$ as a function of the nondimensionalized wave vector qa at times $t = 60$ s (□), 180 s (○), 600 s (△), 900 s (▽), and 1800 s (◇) after the initiation of gelation.

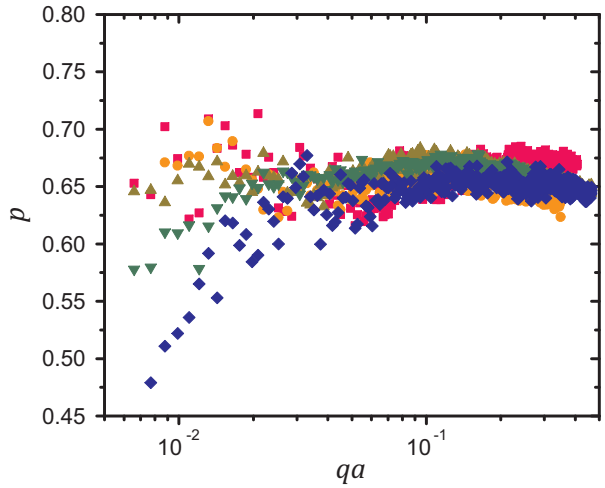

FIG. 3. Stretching exponent p of the aged gels in quasi-steady states as a function of the nondimensionalized wave vector qa at $\phi = 0.5\%$ (□), 0.8% (○), 1.0% (△), 1.5% (▽), and 2.0% (◇).

Eq. (5) can be simplified to our model in Eq. (2) for $q^2\delta^2 \ll 1$, and we find that indeed the values of τ in the two models agree well with each other in the intermediate-q domain, where $q < \sqrt{1/\delta^2}$, as displayed in Fig. 5. For the Krall-Weitz model, τ retains its q-independence up to higher values of q than our model, since q^2 in Eq. (5) effectively decreases the characteristic time scale of the outer exponential as q increases. Yet, for the highest accessible q domain, τ in the Krall-Weitz model also decreases with increasing q. Likewise, the values of δ^2 extracted from the two models closely agree with each other in the intermediate-q domain, while in the highest-q domain δ^2 decreases with q, as shown in Fig. 6. The q-dependence of τ and δ^2 confirms the deviation of the high-q dynamics from the cluster-dominated fluctuations.

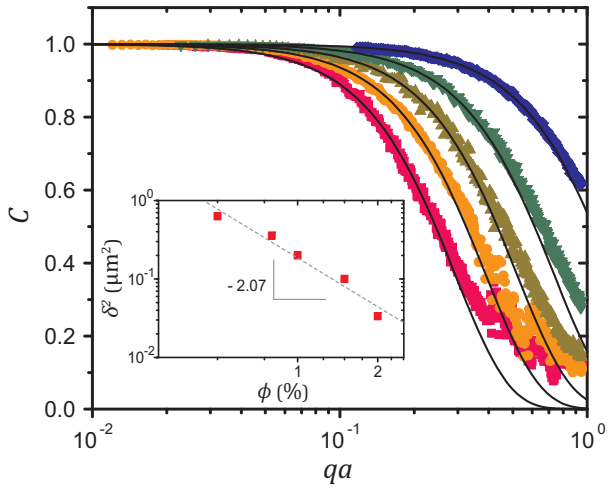

FIG. 4. Nonergodicity parameter C of the aged gels in quasi-steady states as a function of the nondimensionalized wave vector qa at $\phi = 0.5\%$ (□), 0.8% (○), 1.0% (△), 1.5% (▽), and 2.0% (◇). Black lines are fits of Eq. (4) to the intermediate-q regimes. Inset: maximum mean squared displacement of the clusters δ^2 as a function of ϕ.

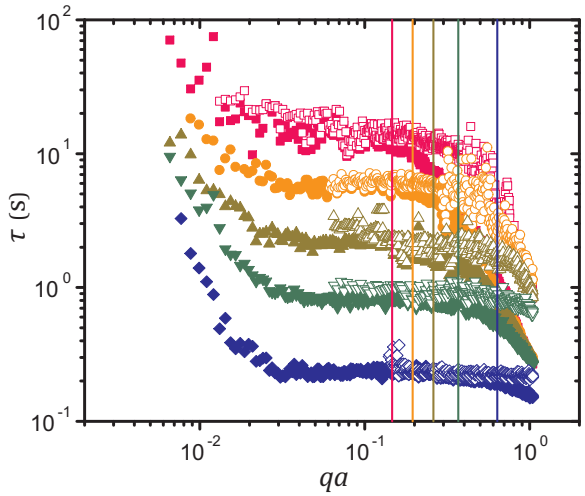

FIG. 5. Relaxation time τ of the aged gels in quasi-steady states as a function of the nondimensionalized wave vector qa at $\phi = 0.5\%$ (□), 0.8% (○), 1.0% (△), 1.5% (▽), and 2.0% (◇). Closed symbols represent the values extracted from our model in Eq. (2) and open symbols from the Krall-Weitz model in Eq. (5). Vertical lines indicate the values of $qa = a\sqrt{1/\delta^2}$, which monotonically increase with ϕ.

We finally investigate the q-dependence of $f(q, \Delta t)$ in the Krall-Weitz model to demonstrate why separate consideration of the characteristic time scale and the nonergodicity, as in Eq. (2), is necessary to capture both the intermediate-q and the high-q dynamics. In the limit of $(\Delta t/\tau)^p \ll 1$, Eq. (5) can be simplified to

$$f(q,\Delta t) \approx \exp\left[-\left(\frac{\Delta t}{(4/\delta^2)^{\frac{1}{p}}\tau q^{-\frac{2}{p}}}\right)^p\right] = \exp\left[-\left(\frac{\Delta t}{\tau^*(q)}\right)^p\right], \tag{6}$$

which leads to the scaling of $\tau^* \sim q^{-2/p}$, given that

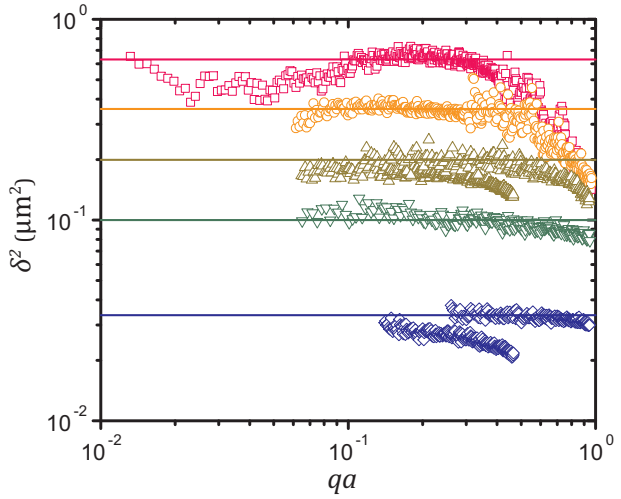

FIG. 6. Maximum mean squared displacement δ^2 of the aged gels in quasi-steady states as a function of the nondimensionalized wave vector qa, extracted from the Krall-Weitz model at ϕ = 0.5% (□), 0.8% (○), 1.0% (△), 1.5% (▽), and 2.0% (◇). Horizontal lines indicate the values of δ^2 at all ϕ obtained from our model as described in Section 6.

both τ and δ^2 are independent of q. Although this result agrees with the q-dependence of the relaxation time of the ergodic subdiffusion in the high-q limit within the model by Reuveni et al. [9], the assumption that $(\Delta t/\tau)^p \ll 1$ when $\tau \sim q^0$ indicates that this scaling has to hold true at any q, if τ is sufficiently large. Thus, we need to account for the q-dependence of the characteristic time scale and that of the nonergodicity separately to properly capture the dynamics in both the intermediate-q domain and the high-q domain.

8. Interpretation of elasticity exponent β

The value of the elasticity exponent $\beta = 2.50 \pm 0.12$ obtained from our analysis in the intermediate-q domain reflects considerable structural rearrangements during the network formation. For a percolating chain resistant to bending and stretching, $\kappa \sim N^{-1} {R_\perp}^{-2}$, where N is the number of particles and $R_\perp$ the radius of gyration of the chain projected onto the plane perpendicular to the line connecting the two ends of the chain [10]. For a chain of end-to-end distance ξ, $N \sim \xi^{d_B}$, where d_B denotes the bond dimension, while $R_\perp \sim \xi^\epsilon$, where ϵ specifies the extent of isotropy of the chain from $\epsilon = 0$ for a perfectly straight chain to $\epsilon = 1$ for an isotropic chain [11]. Consequently, the following scaling relation holds [11, 12]:

$$\kappa \sim \xi^{-(2\epsilon + d_B)} \sim \xi^{-\beta}. \tag{7}$$

The elasticity of a network of fractal aggregates, therefore, is largely conferred by the geometry of the force-bearing backbones. For an ideal network of compactly packed fractal clusters, $\epsilon \approx 1$. Substituting $\beta = 2.50 \pm 0.12$ and the representative value of d_B = 1.1 [13] into Eq. (7), however, we find $\epsilon = 0.70 \pm 0.06$, implying significant anisotropy of the stress-bearing strands. In Fig. 4(c) of the main text, we confirm the prevalence of voids present among the fractal clusters, caused by structural rearrangements that deflect the gel backbones to be anisotropic.

[1] D. C. E. Calzolari, I. Bischofberger, F. Nazzani, and V. Trappe, J. Rheol. **61**, 817 (2017).
[2] N. Dingenouts, C. Norhausen, and M. Ballauff, Macromolecules **31**, 8912 (1998).
[3] F. Giavazzi and R. Cerbino, J. Opt. **16**, 083001 (2014).
[4] F. Giavazzi, P. Edera, P. J. Lu, and R. Cerbino, Eur. Phys. J. E **40**, 97 (2017).
[5] D. C. Johnston, Phys. Rev. B **74**, 184430 (2006).
[6] P. J. Lu, F. Giavazzi, T. E. Angelini, E. Zaccarelli, F. Jargstorff, A. B. Schofield, J. N. Wilking, M. B. Romanowsky, D. A. Weitz, and R. Cerbino, Phys. Rev. Lett. **108**, 218103 (2012).
[7] M. Carpineti and M. Giglio, Phys. Rev. Lett. **68**, 3327 (1992).
[8] A. H. Krall and D. A. Weitz, Phys. Rev. Lett. **80**, 778 (1998).
[9] S. Reuveni, J. Klafter, and R. Granek, Phys. Rev. Lett. **108**, 068101 (2012).
[10] Y. Kantor and I. Webman, Phys. Rev. Lett. **52**, 1891 (1984).
[11] R. de Rooij, D. van den Ende, M. H. G. Duits, and J. Mellema, Phys. Rev. E **49**, 3038 (1994).
[12] S. Romer, H. Bissig, P. Schurtenberger, and F. Scheffold, Europhys. Lett. **108**, 48006 (2014).
[13] P. Meakin, I. Majid, S. Havlin, and H. E. Stanley, J. Phys. A **17**, L975 (1984).